15th AIAA Computational Fluid Dynamics Conference
11-14 June 2001 Anaheim, CA

01-31079

AIAA-2001-2589

AIRWAKE SIMULATIONS ON AN LPD 17 SHIP

Anupam Sharma* and Lyle N. Long†
Department of Aerospace Engineering
The Pennsylvania State University
University Park, PA 16802, U.S.A.

The flow over the *San Antonio* class LPD 17 ship is simulated using Computational Fluid Dynamics (CFD) and parallel computers. Both steady-state and time-accurate results are presented for two yaw cases. The computations are done for inviscid flow with no turbulence modeling. Although the flow is highly turbulent and boundary layer effects may not be insignificant, the essential features, such as vortex shedding, are captured in these simulations because the body has sharp edges. Time accurate simulations are performed for up to 200,000 time steps. The steady state solution is obtained by time averaging the time accurate data, or by running the code in pseudo-time. The steady-state solution and the frequency spectrum are compared with the wind tunnel experiments and are found to be in good agreement. The dominant Strouhal number is found to be of the order unity.

Introduction

THE increasing use of helicopters in conjunction with ships presents the need to accurately predict the abnormal behavior of a helicopter when operated in proximity to a ship. The ship-helicopter dynamic interface offers a multitude of challenges.[1] "Blade Sailing" is one of such problems of paramount importance. The blade-sailing phenomenon is commonly observed when operating a helicopter from a ship deck. In severe conditions blade sailing may result into catastrophic "tunnel-strike" which can severely damage the rotor blades and also cost lives. These problems occur during the take-off and landing phases of the flight of a helicopter, when the centrifugal forces are small. The weak centrifugal force cannot offer enough resistance to the impulsive lift/drag force which can cause large-amplitude oscillations of the blades in longitudinal/lateral direction. The problem is aggravated when operating from a ship deck because of the flow separation from the sharp edges of the mast, the deck and the hangar. The shedding of vortices from the edges characterizes the time variation of the flow over the deck. There is a chance that the shedding frequency will match the angular frequency of the rotor and excite the blades in resonance. This may amplify the deflections to such a level that it strikes the tail boom - "tunnel strike". The problem of blade sailing is particularly addressed by Newman.[2]

Keller and Smith[3] and Keller[4] attempted to model the velocity distribution over the deck using simple linear models. They concluded that such simplified models cannot accurately predict the severe blade sailing observed in practice. This presents the need to obtain the 'real' airwake data either experimentally or numerically.

Until recently, preventive experimental measures have been used to study safety issues. The idea is to locate the safest regions on the ship deck where landing/take-off operations should be performed. Thorough experimental investigations are performed to identify Ship Helicopter Operating Limits (SHOLs) for each ship-helicopter combination. A helicopter can consistently operate safely from within a region called safe-operating envelope, which is bounded by these SHOLs. The process of determining these envelopes is both slow and expensive. The determination of these envelopes for each ship-helicopter combination may cost between $75,000 - $150,000. Besides, the SHOLs significantly change with the conditions at sea, and hence the 'safe' envelopes may not necessarily be safe in all conditions. There are various other problems associated with obtaining experimental data in adverse conditions - when the sea is rough, or when it's very windy. Above all, the data obtained in such conditions cannot be accepted with confidence since there are so many variables.

An alternative to this laborious process is to numerically obtain the ship airwake and use that with some dynamic model of a rotor to predict the blade response. This idea is appealing as it significantly reduces the cost and time. It is time-efficient because once the time-accurate data for the ship airwake is available, it can be used with any helicopter model to obtain the response in minutes. The challenge however is to simulate the flow accurately in time. This has motivated

*Graduate Student, Pennsylvania State University. axs455@psu.edu
†Professor, Assoc. Fellow, AIAA. lnl@psu.edu.

the CFD community to simulate the ship airwake using parallel computers. The first difficulty is to deal with the complicated geometry of the ship. There is no definite length-scale which can be used for such geometries, which further complicates the problem. The biggest challenge still remains to be the lack of computational power. Even with today's powerful parallel computers, computationally intensive jobs like these take days or even months to complete.

A number of attempts have been made to numerically simulate the helicopter/ship dynamics. Healy[5,6] and Johns and Healy[7] addressed the problems with shipboard rotors and looked into the prospects of simulating the ship-helicopter dynamic interface. Healy concluded that the simulation of the airwake is the most challenging and computationally intensive task in this problem. Healy [5] also highlighted the need for more accurate experimental data on real ships. Liu and Long,[8] Tattersall, Albone and Allen[9] and Tai[10] have independently approached the problem of simulating ship airwake. These references suggest different numerical techniques for such simulations.

The present study reports the results of simulations of the LPD 17 ship airwake, and comparison with the wind tunnel experiments. The simulations are performed for two yaw cases. Both steady state and time accurate results are compared. The frequency spectra are compared with the experiments to estimate the Strouhal number of the flow. An extensive comparison is made for the 0° yaw case and the results from the simulations of the 30° yaw case are presented too.

Governing Equations

The Euler equations are solved by neglecting the body forces and using no turbulence modeling. The Euler equations, Eqs. 1, 2 and 3 are written in the integral form and solved using a finite volume formulation.

$$\frac{\partial}{\partial t}\oint_{\mathcal{V}} \rho \mathrm{d}\mathcal{V} + \oint_{S} (\rho\vec{u}).\mathrm{d}\vec{S} = 0 \tag{1}$$

$$\frac{\partial}{\partial t}\oint_{\mathcal{V}} \rho\vec{u} \mathrm{d}\mathcal{V} + \oint_{S} (\rho\vec{u})\vec{u}.\mathrm{d}\vec{S} + \oint_{S} p\mathrm{d}\vec{S} = 0 \tag{2}$$

$$\frac{\partial}{\partial t}\oint_{\mathcal{V}} \rho E \mathrm{d}\mathcal{V} + \oint_{S} (\rho E + p)\vec{u}.\mathrm{d}\vec{S} = 0 \tag{3}$$

The system is closed by the equation of state for an ideal gas.

$$p = \rho R T \tag{4}$$

In the above, S denotes the surface of the control volume $\mathcal{V}$. Overhead vector, ($\vec{}$) is used to represent vector quantities. p is pressure, ρ is fluid density, T is temperature, $\vec{u}$ is velocity, E is the energy per unit mass and R is the universal gas constant.

Since no turbulence modeling is used, the smallest turbulent scales that are captured in these simulations are of the order of the grid size. Boundary layer effects are ignored by making the inviscid flow approximation. The sharp edges of the boundary should make the flow fairly Reynold's number independent.

Parallel Machines

A sequential computation of such a complicated flow is not possible due to CPU time constraints. Parallel processing is used to accelerate the simulation process. All the computations referred to in this paper have been performed in parallel. Three facilities offering parallel computational power at Penn State have been used for all computations - COst effective COmputing Array (COCOA),[11,12] COCOA2 and LionX.[13] COCOA has been primarily used to generate the results presented in this paper.

COCOA is a Beowulf cluster with 25 nodes each having dual 400 MHz Pentium II processors. This facility was assembled by the authors and their colleagues in the Department of Aerospace Engineering at Penn State. The machines are connected via fast-Ethernet network which can support up to 100 Mbps bandwidth. A single Baynetworks 24-port fast-Ethernet switch with a backplane bandwidth of 2.5 Gbps is used for the networking. All the processors are dedicated to run parallel jobs. The operating system is Red Hat Linux. Message Passing Interface (MPI) is used for parallel programming and the Gnu C compiler is used for compiling PUMA. Details regarding setting up and benchmarking of COCOA may be obtained from Modi and Long[11] and COCOA's website.[12]

COCOA was primarily set up to make parallel computing facility readily available to the CFD group of the Aerospace Engineering Department at Pennsylvania State University. The total cost of the cluster was just $80,000 in the year 1998, when it was set up. Since then this facility has been intensively used for various CFD simulations. COCOA2 is a newly assembled Beowulf cluster at Penn State. It has 21 nodes each having dual 800 MHz Pentium III processors and 1 GB RAM each. The cluster has dual fast-Ethernet per node and all the nodes are connected using two HP2524 switches with channel bonding.

LionX is also a Beowulf cluster with 32 machines (each having dual 400 MHz Intel Xeon processors). These machines are connected via Myricom Myrinet with wire speed 1.28 Gbps. LionX also uses Linux with MPI for parallel programming. Performance comparison and benchmarking results for LionX can be obtained from its website.[13]

The Flow Solver - PUMA

The Parallel Unstructured Maritime Aerodynamics (PUMA)[11,14–16] code is a computer program written

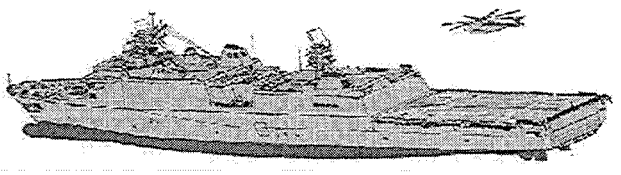

Fig. 1 The port out-board profile of LPD 17.

in C for the analysis of internal and external non-reacting compressible flows over arbitrary complex geometries. PUMA uses Message Passing Interface (MPI) to run the code in parallel. It can be run on arbitrary number of processors with very good scaling performance. Modi and Long,[11] Modi,[14] Bruner and Walters[15] and Long, Souliez and Sharma[16] detail the benchmarking of the performance, and validation of PUMA.

PUMA is based on the finite volume method and supports mixed topology unstructured grids composed of tetrahedra, wedges, pyramids and hexahedra. The code may be run to preserve time accuracy for unsteady problems, or may be run using a pseudo-unsteady formulation to enhance the convergence to the steady state. Primitive flow quantities are computed at the cell centers. The code can be restarted from previous computations. All flow variables are stored with double precision, but may be optionally stored as single precision to save memory and time for message passing, at the cost of reduced precision. PUMA has been used for all computations referred to in this paper.

The Unstructured Grid

The San Antonio LPD 17 (Fig. 1) is the US Navy's newest class of ship. It is a warfare capable ship but its primary mission is the amphibious transport of marines and cargo. The prominent features which mark the geometry of LPD 17 are the two masts one behind the other separated by a distance of about 90 m.

For a complicated geometry like the LPD 17, an unstructured grid is the obvious choice. The grid used for the simulations was generated using Gridgen.[17] Figure 2 shows the grid point distribution over the surface of the ship. Clustering is done all around the ship with increasing cell size towards the boundaries of the bounding box. The computational domain extends to a distance of $2L$ both in front and behind the ship, where $L = 200$ m is the ship length. The side outer boundaries are at a distance of $7 \times W$ from the center plane, where $W = 30$ m is the width of the ship deck. The waterline is taken to be the bottom surface of the bounding box. The upper outer boundary is at a distance of $6 \times H$ from the waterline, where $H = 50$ m is the maximum height of the ship. Figure 3 shows the size of the bounding box in relation to the size of the ship.

All the computations are performed for inviscid flow.

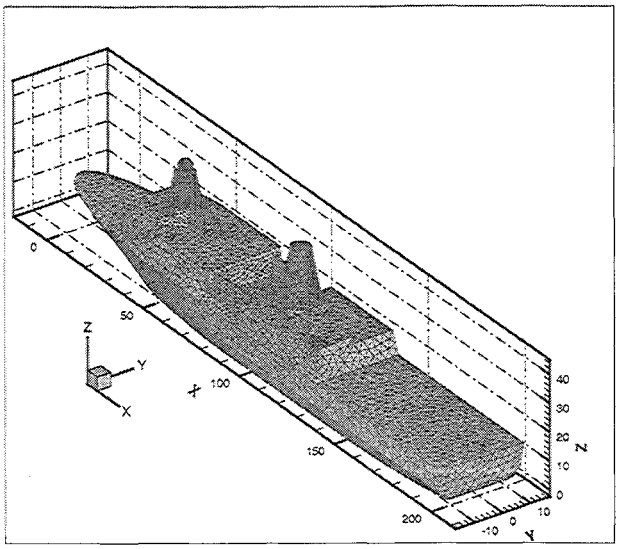

Fig. 2 The surface grid on the LPD 17 generated using GridGen.[17]

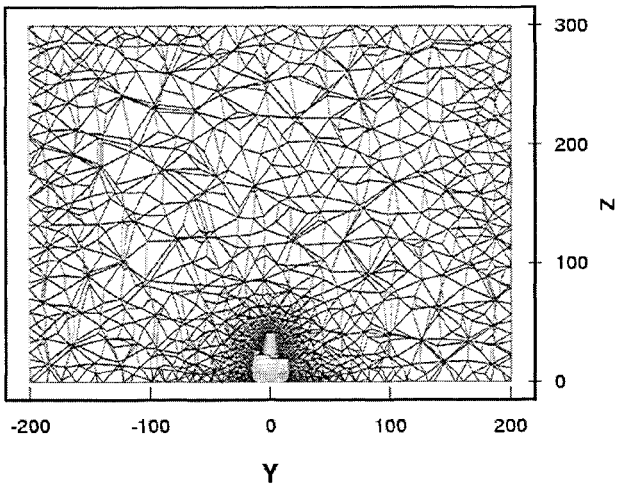

Fig. 3 A slice of the volume grid at $X = 108$ m.

Hence, the only boundary condition imposed at the ship surface is that the velocity normal to the surface is zero. The waterline which is the bottom face of the bounding box is also assigned the zero-normal-velocity condition. All the other faces of the bounding box are assigned the Riemann boundary condition to avoid any reflections into the domain.

Since the time step for time-accurate computations (using an explicit scheme) is determined by the smallest cell in the volume grid, a fairly uniform surface grid is chosen (Fig. 2). The total number of tetrahedra in the volume grid is around 0.2 million. The minimum cell length is about 7 mm which gives a time step of 6×10^{-5} seconds for a Courant-Friedrichs-Lewy (CFL) number of 0.8.

Simulations and Comparison with the Experiments

Two cases have been studied : 0° head wind, and a cross wind at a yaw angle of 30° to the ship. The yaw angle is defined as the angle the velocity vector makes with the center plane of the ship. Since the ship is aligned with the X axis in the simulations, the yaw angle is just the angle between the X axis and the velocity vector. The positive X axis is chosen to point towards the rear from the bow of the ship. The positive Z axis points vertically up, and the Y axis forms a right-handed coordinate system. The origin is located at the point where the bow of the ship intersects the waterline.

For both cases the magnitude of the freestream velocity is 30 kts. (15.44 m/s). In order to achieve a reasonable (i.e. computationally efficient) Mach number, the freestream pressure value is reduced to 5.2 KPa. With reduced pressure, and freestream air density of 1.226 kg/m^3, the speed of sound is 77 m/s. The Mach number is thus scaled by a factor of 4. It is well known that low Mach number flows are fairly insensitive to Mach number.

All the domain cells are initialized with freestream values. Once the initial conditions are specified, the boundary conditions and the geometry of the ship govern the flow. Flows over bluff bodies like a ship never reach a steady state. The flow pattern keeps changing with time. This change may be periodic or aperiodic, depending on the Reynolds number of the flow. For very high Reynolds number flows, as is the case here, the flow is turbulent and hence aperiodic. The vortices are shed from the bow, the masts, the hangar and other objects protruding from the surface of the ship. It is nearly impossible to analytically estimate the frequencies which would dominate the time variation of the flow over the deck. The aim of these computations is to accurately predict these frequencies and to predict the large scale flow structures.

The experiments were conducted by the Naval Surface Warfare Center (Carderock divison)[18] . The experimental model was scaled down by a factor of 94 to accommodate the wind tunnel. Time accurate data was collected at a few points above the deck for two yaw values : 0° and 30°. The sampling rate was 0.02 seconds. Figure 4 shows the location of the points at which the experimental data was collected for the 0° yaw case.

Pseudo Steady State

Local time stepping (pseudo time marching) is used with the Successive Symmetric Over Relaxation (SSOR) scheme to accelerate the convergence to a physically realistic flow. Since there is no fixed steady-state, a physically realistic solution at any point of time is referred to as a "pseudo steady state". It requires about 600 iterations, which take 6 hours of wall-time on 8 processors of COCOA, to reach a "pseudo steady state". A "pseudo steady state" is a good representative of the time averaged solution. The analysis of a "pseudo steady state" solution can reveal important information about the 'static' flow field.

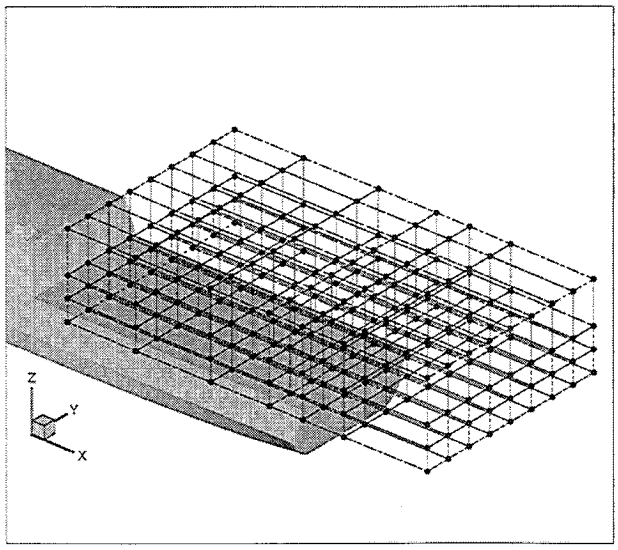

Fig. 4 The points at which experimental data is collected for the 0° yaw case.

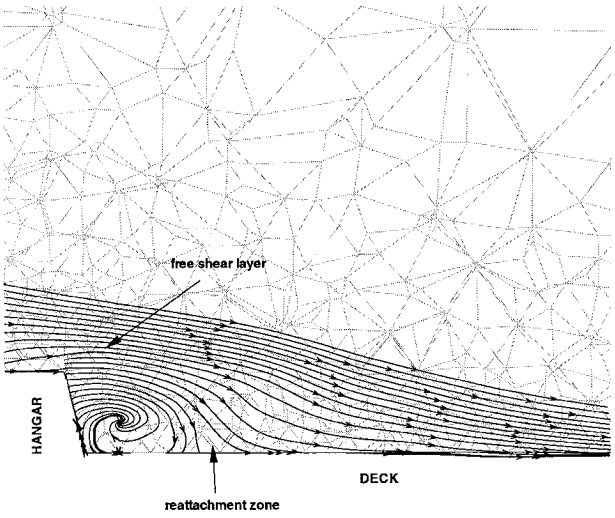

Fig. 5 Recirculation and re-attachment behind the hangar.

Figures 5 and 6 show the streamlines for the "pseudo steady state" solution for the 0° yaw case behind the hangar and between the two masts, respectively. The figures clearly show the recirculation. The flow over the hangar is very similar to the flow over a backward facing step. It exhibits the separation of the shear layer and its re-attachment downstream (Fig. 5).

Figures 7 and 8 show the contour plots of the velocity magnitude and the coefficient of pressure (C_p) for the 0° yaw case. The plots are drawn at the center plane (Y=0). Figures 9 and 10 show similar plots for

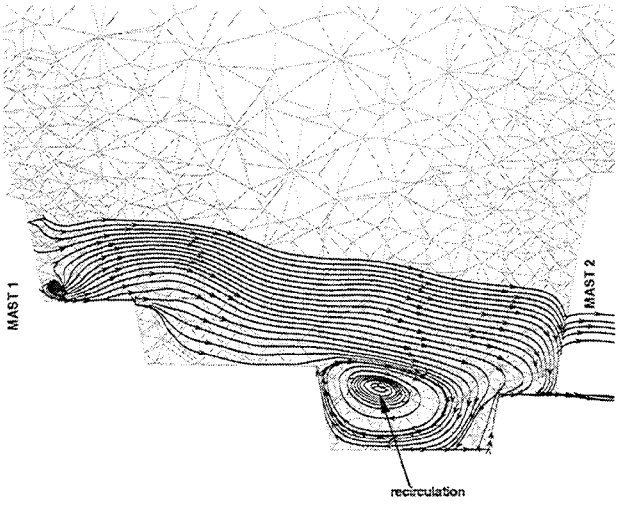

Fig. 6 Recirculation in between the two masts.

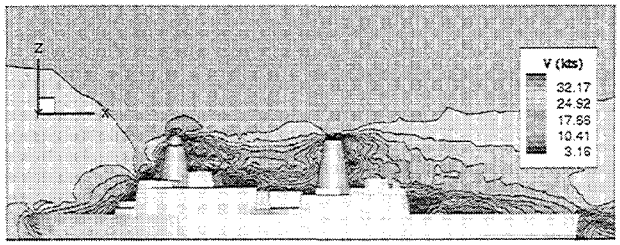

Fig. 7 Velocity contours at the center plane (Y=0) for the 0° yaw case (pseudo steady-state).

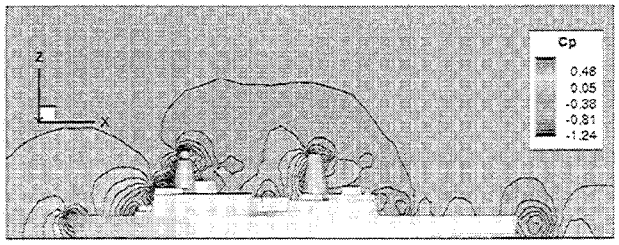

Fig. 8 C_p contours at the center plane (Y=0) for the 0° yaw case (pseudo steady-state).

the 30° yaw case. Since the stagnation points do not lie on the $Y = 0$ plane for a non-zero yaw case, the C_p is low in front of the masts (Fig. 10). A similar trend is observed in the velocity contour plot (Fig. 9); high velocity in front of the masts due to the curvature.

The velocity contours are plotted for both yaw cases on a $Y - Z$ plane at $X = 153$ m (Figs. 11 and 12) to study the effect of yaw on the flow pattern in the lateral direction. This plane is located 15 m behind the hangar. The velocity contours clearly show the drift of the wake in the direction of velocity. For the 30° yaw case, the ship deck behaves like a forward facing step and a backward facing step in a tandem arrangement for the lateral velocity component.

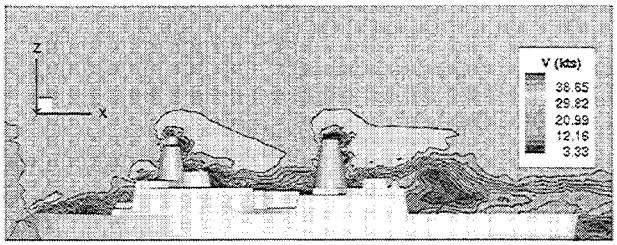

Fig. 9 Velocity contours at the center plane (Y=0) for the 30° yaw case (pseudo steady-state).

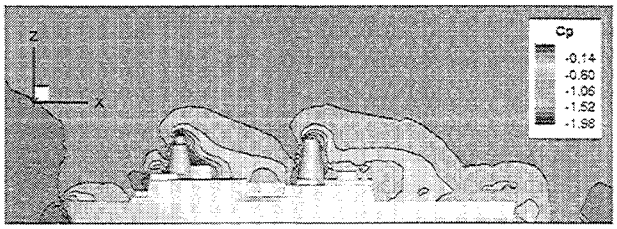

Fig. 10 C_p contours at the center plane (Y=0) for the 30° yaw case (pseudo steady-state).

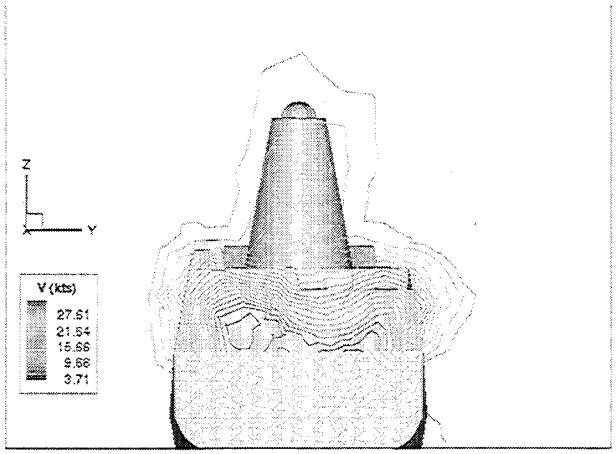

Fig. 11 Velocity contours at $X = 153$ m for the 0° yaw case (pseudo steady-state).

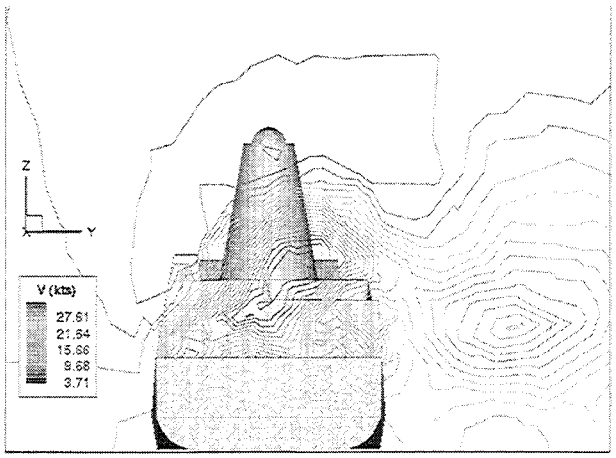

Fig. 12 Velocity contours at $X = 153$ m for the 30° yaw case (pseudo steady-state).

Time Accurate Simulations

While the pseudo steady state solution provides a snapshot of the flow-field, it does not contain any time dependent information, like vortex shedding frequency etc. Time accurate simulations are essential to capture the dynamics of the flow over the deck.

An unstructured grid is not a perfect choice for time-accurate simulations, as it generates a few very small cells which drastically reduce the time step of integration. For explicit schemes, the time step cannot be arbitrarily increased by increasing the CFL because of stability concerns. The wall-time for simulating 1 second of real flow increases with decreasing cell size. Hence the computations become extremely time consuming. Further clustering of the grid in order to accurately resolve the flow increases the time cost in two ways : (1) the number of cells increase i.e. wall-time per iteration increases, and (2) the smallest cell size reduces i.e. the time step reduces. The cell-size variation is therefore as important as the number of cells in the grid.

Although the unstructured grid does present some problems, the alternative of using a structured grid over an extremely complicated geometry like LPD 17 is infeasible. Hence, the same unstructured grid (Fig. 2) is used for the time accurate computations. The CFL is kept constant at 0.8 which gives a timestep of 6×10^{-5} s. The time accurate computations are started from a "pseudo steady state" solution. It takes around 17,000 iterations to simulate 1 s of real flow, and requires about 2 days on 8 processors of COCOA.

In order to compare the numerical results with the experiments, the primitive flow variables are nondimensionalized as follows:

$$\tilde{u} = u/V_\infty \ ; \ \tilde{v} = v/V_\infty \ ; \ \tilde{w} = w/V_\infty$$
$$\tilde{p} = p/p_\infty \ ; \ \tilde{t} = t/T_s \ ; \ St = 1/\tilde{t}.$$

where the ($\tilde{}$) quantities are the nondimensional variables, ∞ represents free-stream values, V is the magnitude of the velocity, p represents pressure, t is time and T_s is the time scale. T_s is calculated by taking the ratio of the length scale (chosen to be the ship length) and the velocity scale, V_∞. The Strouhal number (St) is the nondimensional frequency. u, v and w are the components of velocity in the X, Y and Z directions respectively.

The freestream velocity is identical in the simulations and the experiments, but the geometry is scaled down by a factor of 94 for the experiments. Using similarity principle, the time scale in the experiments should be 94 times smaller than the time scale in the simulations.

The experimental data is available for 40 seconds of real time which is equivalent to 290 units of nondimensional time. The simulations are performed for 10 seconds which is equivalent to 1 unit of nondimensional time. It is known from the experiments that the typical Strouhal number for the problem is about unity. Therefore, simulations done for a unit nondimensional time may capture the flow dynamics. Simulation of 1 unit of nondimensional time takes approximately a month of computations on 8 processors of COCOA. With this speed, it would take years to simulate 290 units of nondimensional time on 8 processors. This quantifies the magnitude of the problem.

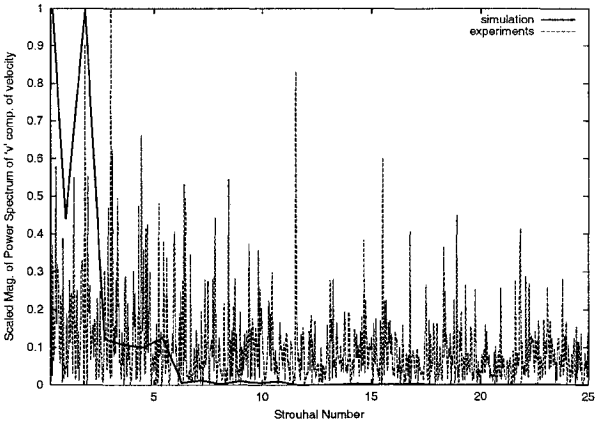

Fig. 13 Frequency Spectrum of 'v' (0° yaw; location - $X = 170$ m, $Y = 0$, $Z = 17$ m).

Since the experimental data has been collected over a considerably longer period of time than the simulated data, it resolves the low-frequency components much more accurately. The sampling rate for the simulations is 7×10^{-5}, whereas for the experiments it is 0.15, in non dimensional time units. Though the simulations should resolve the high-frequency components better than the experiments, it is not neccessarily the case here as the small scale turbulence is not captured by the simulations.

Figures 13, 14 and 15 show the frequency spectra of v, w and $|V|^2$ respectively, at a point on the centerplane behind the hangar, for the 0° yaw case. The magnitude of the power spectra is scaled by the peak value between St = 0.2-25. Figures 16, 17 and 18 plot the frequency spectra of the same variables at a different point, for the 30° yaw case. Although the simulations do not capture the low-frequency components accurately, they clearly indicate that the dominant frequencies lie between $St = 1 - 3$.

Time-Averaged Solution

It has been argued that a "pseudo steady state" solution does not match well with the time-averaged experimental results,[19] while the data obtained on time averaging the time accurate simulations matches fairly well. A comparison between a "pseudo steady state" solution and the time averaged solution is made to examine if this is true for the case in the present study. The time accurate data is sampled for a unit nondimensional time.

Figures 19 and 20 show the velocity contours of the

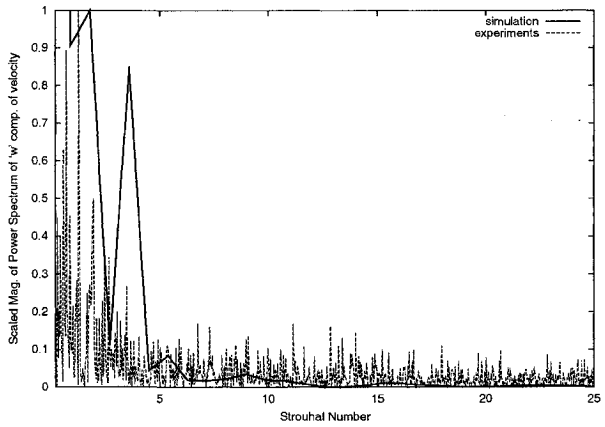

Fig. 14 Frequency Spectrum of 'w' (0° yaw; location - $X = 170$ m, $Y = 0$, $Z = 17$ m).

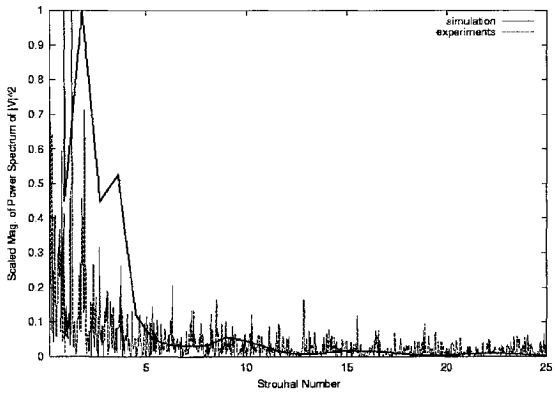

Fig. 15 Frequency Spectrum of $|V|^2$ (0° yaw; location - $X = 170$ m, $Y = 0$, $Z = 17$ m).

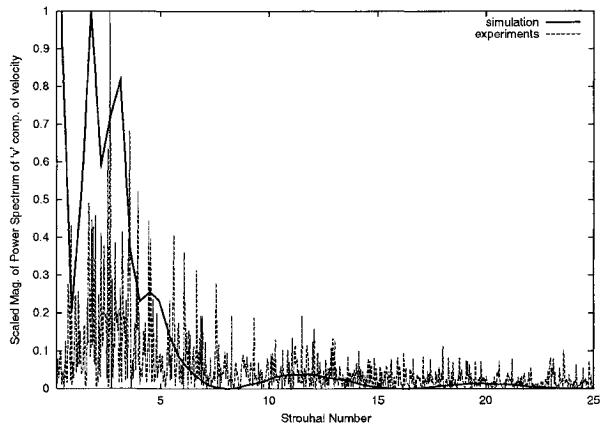

Fig. 16 Frequency Spectrum of 'v' (30° yaw; location - $X = 170$ m, $Y = 0$, $Z = 25$ m).

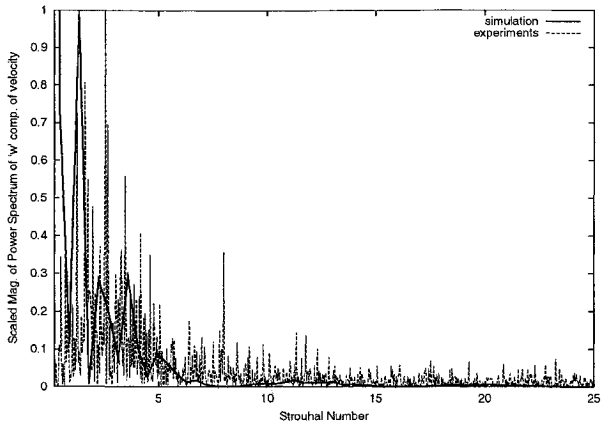

Fig. 17 Frequency Spectrum of 'w' (30° yaw; location - $X = 170$ m, $Y = 0$, $Z = 25$ m).

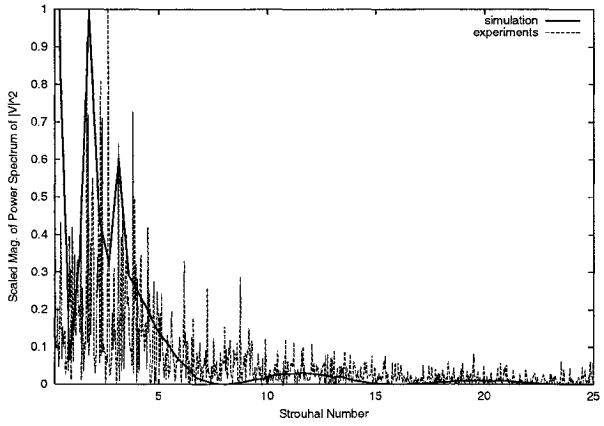

Fig. 18 Frequency Spectrum for $|V|^2$ (30° yaw; location - $X = 170$ m, $Y = 0$, $Z = 25$ m).

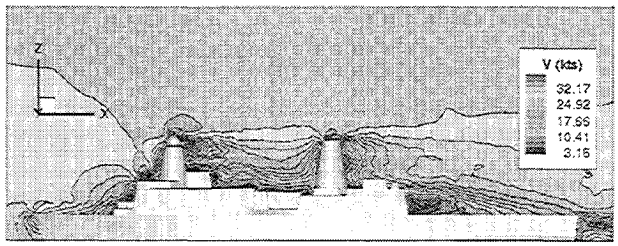

Fig. 19 Velocity contours at the center plane (Y=0), for the 0° yaw case (simulated time-averaged solution).

time averaged solution at the center plane for 0° yaw and 30° yaw, respectively. Comparison of Figs. 7 and 19, and 9 and 20 shows that a "pseudo steady state" solution represents the time averaged solution fairly well. This might be due to our use of an explicit scheme. Previous studies[19] have used implicit methods. Implicit schemes permit larger time steps to be used (since they are more stable), but this often means that the small cells will have very large local CFL numbers. There may be a loss of accuracy due to this which may account for their difference between pseudo-time and time-averaged solutions.

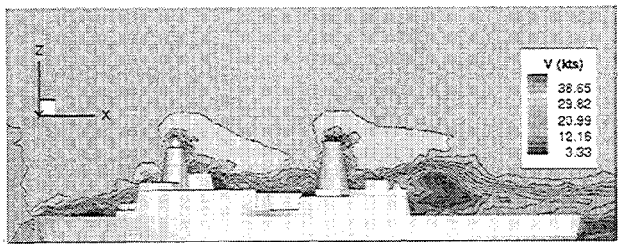

Fig. 20 Velocity contours at the center plane ($Y = 0$) for the 30° yaw case (simulated time-averaged solution).

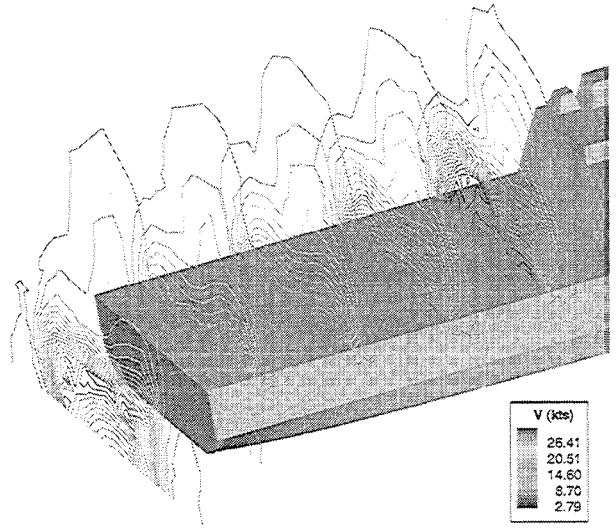

Fig. 21 Velocity contours at $X = 150, 165, 180, 195$ and 210 m for the 0° yaw case (simulated time-averaged solution).

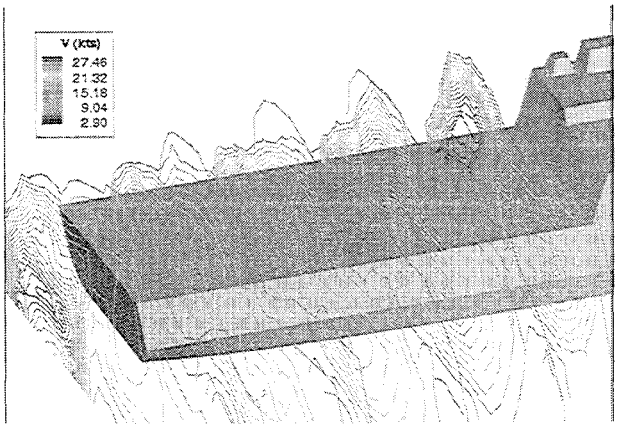

Fig. 22 Velocity contours at $X = 150, 165, 180, 195$ and 210 m, for the 30° yaw case (simulated time-averaged solution).

Figures 21 and 22 show the velocity contours of the time averaged solution for 0° yaw and 30° yaw, respectively, at a few X locations on the deck. The asymmetry in the wake, even for the 0° yaw case, is apparent in the figures. This is expected as the ship is not symmetric about the $Y = 0$ plane.

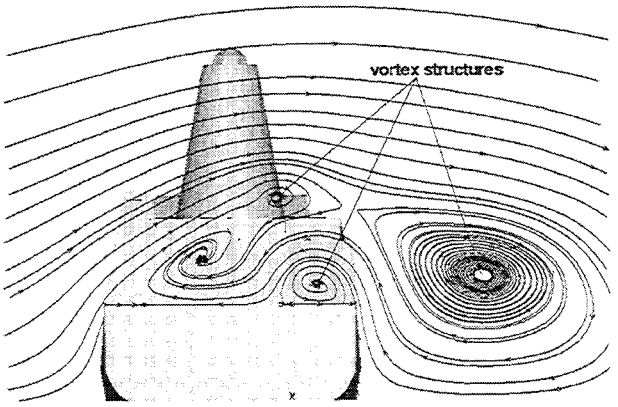

Fig. 23 Surface streamlines on $X = 153$ m plane, for the 30° yaw case (simulated time-averaged solution).

In the time averaged solution for the 30° yaw case (Fig. 22), a vortex structure can be seen detached from the deck aligned in the direction of the wind. Figure 23 shows the surface-streamlines plot on the $X = 153$ m plane. The vortex structure is clearly seen in the figure. These structures are continuously generated and shed in time.

Figures 24 and 25 compare the time averaged data obtained from simulations with the experiments. The simulations are in agreement in capturing the wake of the hangar, although there is more asymmetry in the simulated result. The simulations also do not clearly show the wake of the second mast as observed in the experiments. This may be due to two effects : first the experimental data is taken only at 36 points on the plane, and hence cannot capture the details, and second, the simulations are done for just 1-2 cycles and hence may contain the effect of shed vortices. Figures 26 and 27 plot the time averaged solution at a few X locations from the simulations and from the experiments, respectively.

Figures 28-36 compare the steady state velocity distribution over the deck with the experiments. The simulations follow the velocity pattern in the experiments but under-predict the wake, especially, behind the hangar (Fig. 28), and near the surface of the ship deck (Fig. 34). This may be because of the inviscid flow assumption, or because of inadequate sampling for obtaining the steady state.

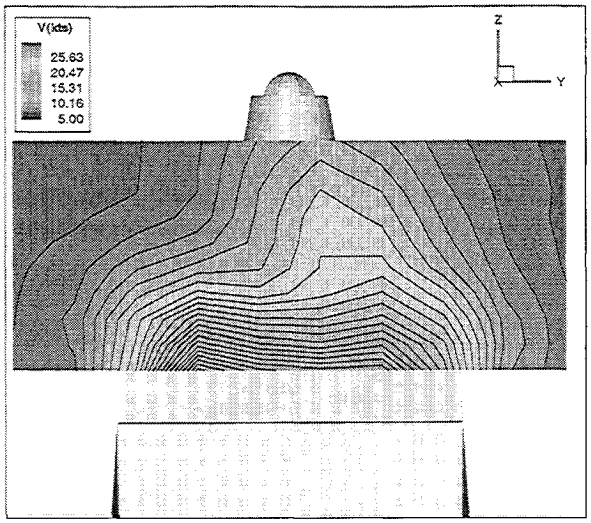

Fig. 24 Velocity contour plot at $X = 165$ m for the 0° yaw case (simulated time-averaged solution).

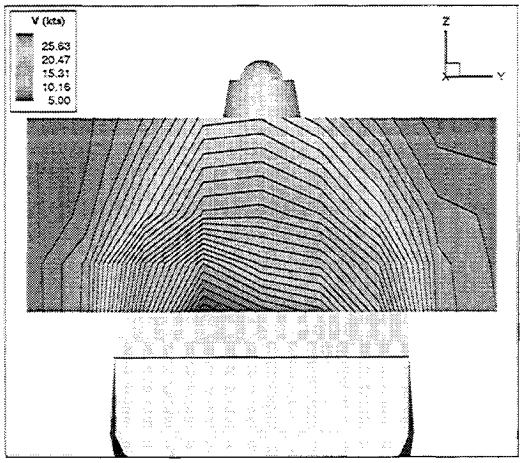

Fig. 25 Velocity contour plot at $X = 165$ m for the 0° yaw case (experimental time-averaged solution).

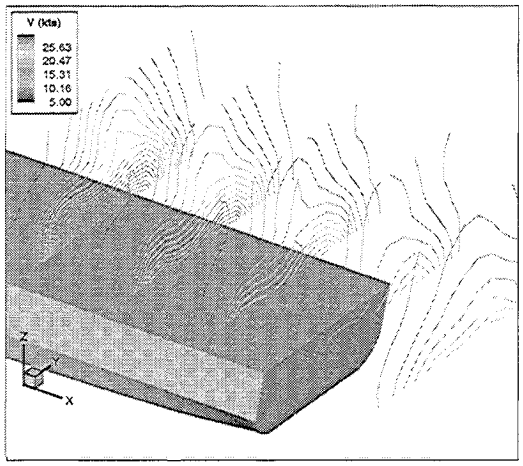

Fig. 26 Velocity contour plots at $X = 165$, 180, 195, 210 and 225 m for the 0° yaw case (simulated time-averaged solution).

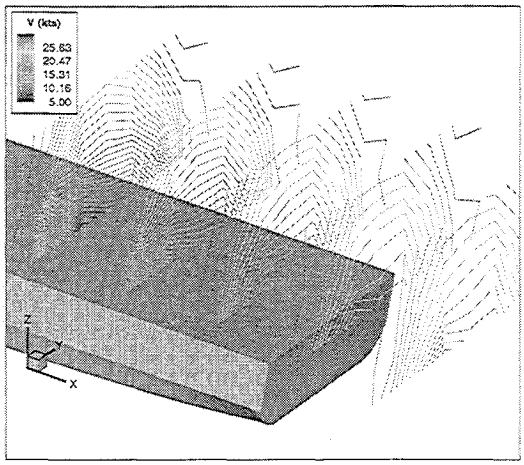

Fig. 27 Velocity contour plots at $X = 165$, 180, 195, 210 and 225 m for the 0° yaw case (experimental time-averaged solution).

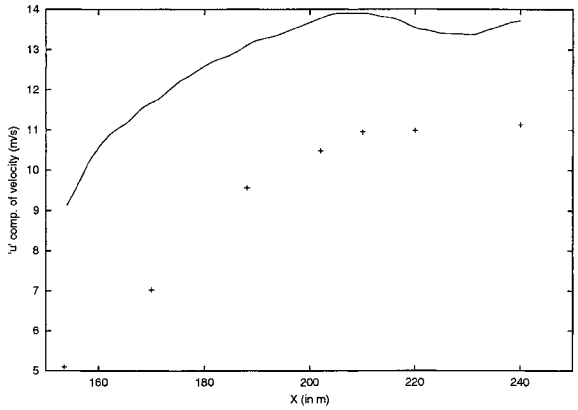

Fig. 28 Longitudinal velocity distribution along the center line ($Y = 0$ and $Z = 22$ m), for 0° yaw (steady-state solution). Solid line - simulations; crosses - experiments.

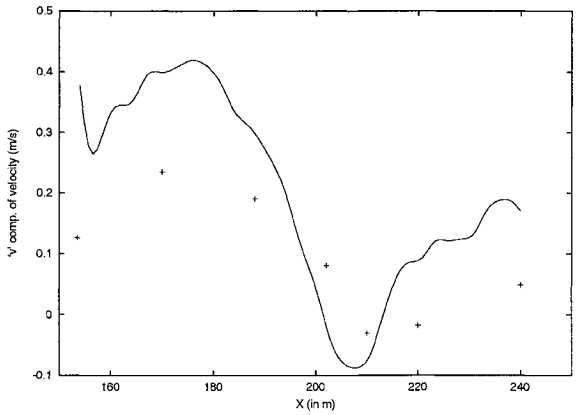

Fig. 29 Transverse velocity distribution along the center line ($Y = 0$ and $Z = 22$ m), for 0° yaw (steady-state solution). Solid line - simulations; crosses - experiments.

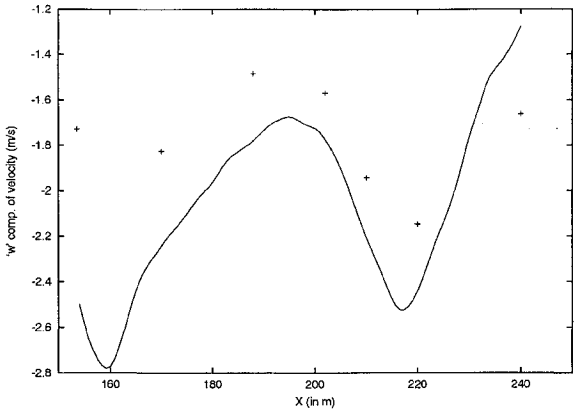

Fig. 30 Vertical velocity distribution along the center line ($Y = 0$ and $Z = 22$ m), for 0° yaw (steady-state solution). Solid line - simulations; crosses - experiments.

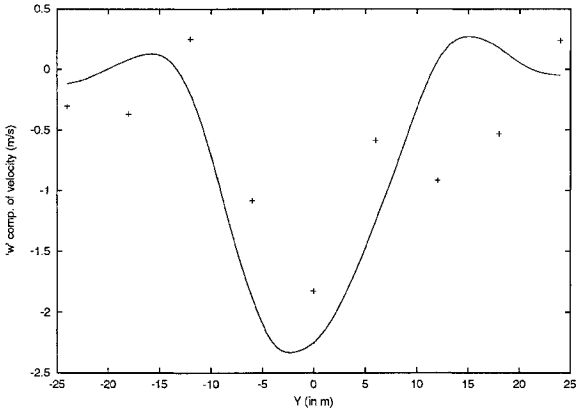

Fig. 33 Vertical velocity distribution across the deck ($X = 170$ m and $Z = 22$ m), for 0° yaw (steady-state solution). Solid line - simulations; crosses - experiments.

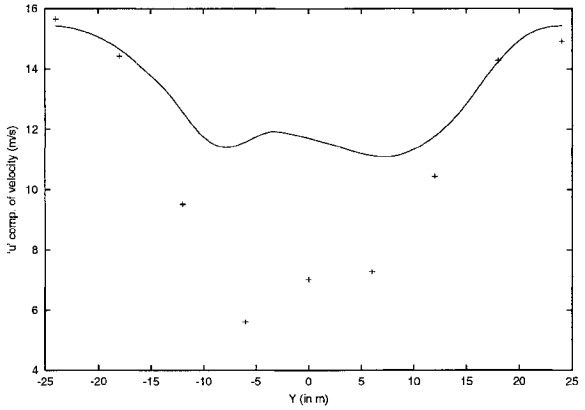

Fig. 31 Longitudinal velocity distribution across the deck ($X = 170$ m and $Z = 22$ m), for 0° yaw (steady-state solution). Solid line - simulations; crosses - experiments.

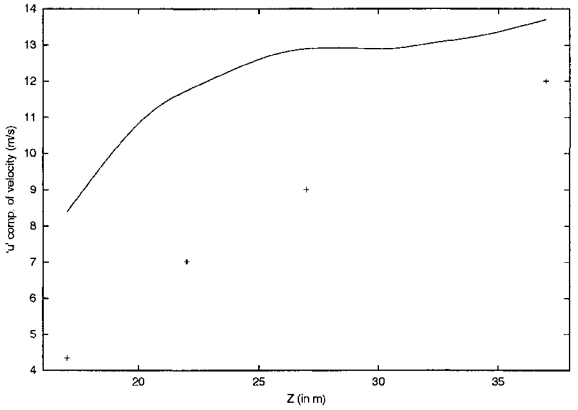

Fig. 34 Longitudinal velocity distribution above the deck ($X = 170$ m and $Y = 0$), for 0° yaw (steady-state solution). Solid line - simulations; crosses - experiments.

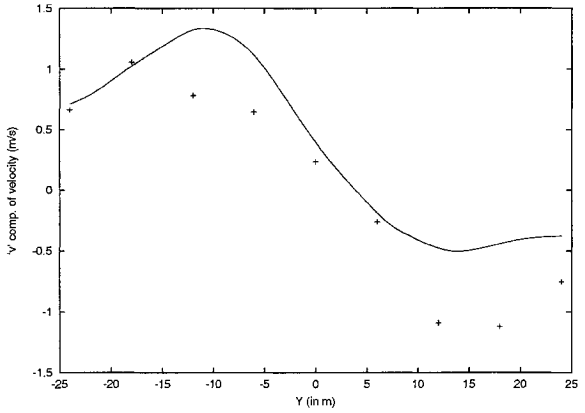

Fig. 32 Transverse velocity distribution across the deck ($X = 170$ m and $Z = 22$ m), for 0° yaw (steady-state solution). Solid line - simulations; crosses - experiments.

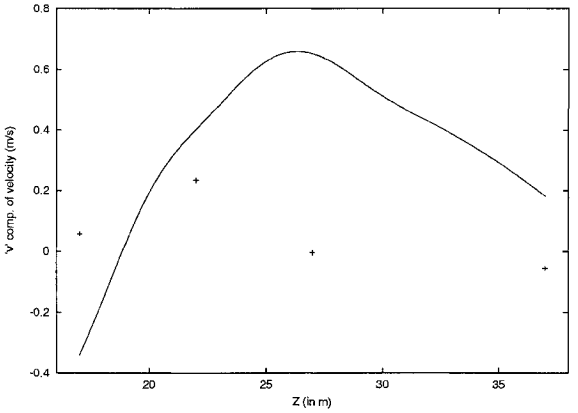

Fig. 35 Transverse velocity distribution above the deck ($X = 170$ m and $Y = 0$), for 0° yaw (steady-state solution). Solid line - simulations; crosses - experiments.

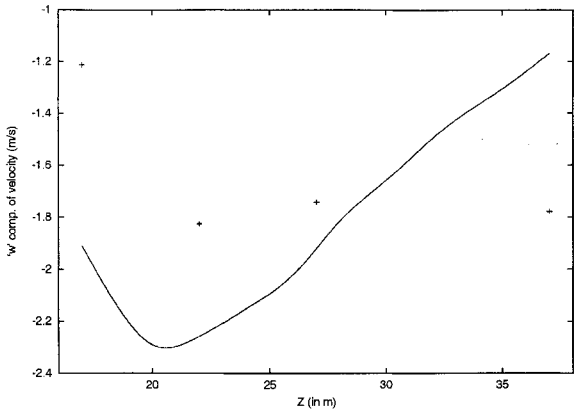

Fig. 36 Vertical velocity distribution above the deck ($X = 170$ m and $Y = 0$), for 0° yaw (steady-state solution). Solid line - simulations; crosses - experiments.

Conclusion

The airwake over the LPD 17 was numerically simulated using parallel machines. Two cases have been simulated : 0° and 30° yaw. The results for both time accurate simulations and the steady state are presented for the two cases. Although there is no steady state for the problem, a "pseudo steady state" is found to represent the general flow pattern over the ship. The time averaged data compares very well with a "pseudo steady state" solution, and fairly well with the experiments. The simulations slightly under-predict the wake which may be because of the inviscid flow assumption.

One unit of nondimensional time is simulated accurately in time. Frequency spectra plots from the simulations are compared with the experiments. The experiments strongly indicate that the dominant Strouhal number is of the order unity; this is supported by the simulations. The need to sample more time-accurate data to accurately resolve the low Strouhal numbers is highlighted. We plan to do longer time-accurate runs. With such limited data it is difficult to pinpoint the Strouhal number in the wake, but the simulations correctly estimate the order of magnitude of the Strouhal number.

Acknowledgments

The authors would like to express gratitude to the U.S. Navy and the University of New Orleans for sponsoring this project. The authors would also like to acknowledge the Naval Surface Warfare Center (Carderock division) for providing us with the experimental data, and Martin Guillot, University of New Orleans, for providing the IGES file of the ship geometry and many helpful suggestions.

References

[1]Lumsden, R. B., Wilkinson, C. H., and Padfield, G. D., "Challenges at Helicopter-Ship Dynamic Interface," 24^{th}European Rotorcraft Forum, 1998.

[2]Newman, S., "The Phenomenon of Helicopter Rotor Blade Sailing," *Proceedings of the Institution of Mechanical Engineers*, Vol. 213, 1999.

[3]Keller, A. J. and Smith, E. C., "Analysis and Control of the Transient Shipboard Engagement Behaviour of Rotor Systems," *American Heliocpter Society* 55^{th} *Annual Forum*, 1999.

[4]Keller, J., *Aeromechanical Analysis and Control of Shipboard Helicopter Rotor Engagements and Disengagements*, Ph.D. thesis, The Pennsylvania State University, Department of Aerospace Engineering, May 2001.

[5]Healy, J. V., "The Prospects for Simulating the Helicopter/Ship Dynamic Interface," *Naval Engineers Journal*, Vol. 99, No. 2.

[6]Healy, J. V., "Simulating the Helicopter/Ship Dynamic Interface as an Alternative to Current Methods of Determining the Safe Operating Limits," *The Naval Air Systems Command*, 1985.

[7]Johns, M. K. and Healy, J. V., "The Airwake of a DD-963 Class Destroyer," *Naval Engineers Journal*, May 1989.

[8]Liu, J. and Long, L. N., "Higher Order Accurate Ship Airwake Predictions for the Helicopter/Ship Interface Problem," American Helicopter Society, 54^{th} Annual Forum, Washington D.C., May 1988.

[9]Tattersall, P., Albone, C. M., Soliman, M., and Allen, C. B., "Prediction of Ship Airwakes over Flight Decks using CFD," A report to the Department of Aerospace Engineering, University of Bristol, UK, 1988.

[10]Tai, T., "Simulation and Analysis of LHD Ship Airwake by Navier-Stokes Methods," NATO RTO Symposium on Fluid Dynamics, Amsterdam, The Netherlands, Oct. 1998.

[11]Modi, A. and Long, L. N., "Unsteady Separated Flow Simulations using a Cluster of Workstations," Paper 2000-0272, 38^{th} Aerospace Sciences Meeting & Exhibit, Jan. 2000.

[12]http://cocoa.ihpca.psu.edu.

[13]http://cac.psu.edu/beatnic/Cluster/Lionx/perf.

[14]Modi, A., *Unsteady Separated Flow Simulations using a Cluster of Workstations*, M.S. thesis, The Pennsylvania State University, Department of Aerospace Engineering, May 1999.

[15]Bruner, C. W. S. and Walters, R. W., "Parallelization of the Euler Equations on Unstructured Grids," AIAA Paper 1997-1894, 35th Aerospace Sciences Meeting, Jan. 1997.

[16]Long, L. N., Souliez, F., and Sharma, A., "Aerodynamic Noise Prediction using Parallel Methods on Unstructured Grids," AIAA Paper 2001-2196, 7^{th} AIAA/CEAS Aeroacoustics Conference, Maastricht, The Netherlands, May 2001.

[17]http://www.pointwise.com/.

[18]Guillot, M. J. and Walker, M. A., "Unsteady Analysis of the Air Wake over the LPD-17," AIAA Paper 2000-4125, 18^{th} AIAA Applied Aerodynamics Conference and Exhibit, Denver, CO, 2000.

[19]Polsky, S. A. and Bruner, C. W. S., "Time-Accurate Computational Simulations of an LHA Ship Airwake," AIAA Paper 2000-4126, 18th AIAA Applied Aerodynamics Conference, Denver, CO, 2000.